VERSITA

POTENTIAL OF AUTORADIOGRAPHY TO DETECT SPATIALLY RESOLVED RADIATION PATTERNS IN THE CONTEXT OF TRAPPED CHARGE DATING

DANIEL RUFER and FRANK PREUSSER

Institute of Geological Sciences, University of Bern, Baltzerstrasse 1+3, 3012 Bern, Switzerland

Abstract: Recent developments in optically stimulated luminescence (OSL) dating allow the determination of signals in increasingly smaller sample amounts. This has led to microdosimetry having a larger impact on equivalent dose (D_E) distributions and therefore, detection and assessment of spatial distribution of radionuclides has become more important. This study demonstrates the application of autoradiography using imaging plates to determine spatially resolved radiation inhomogeneities in different types of samples. Qualitative evaluations of radiation inhomogeneity are carried out on unconsolidated sediments as well as on hard rock samples. While indicating some limitations of applicability, the results demonstrate that the method is an efficient tool to detect and document spatial variations in a sample's radiation field. It therefore provides a possibility to rapidly screen samples to check whether microdosimetry might affect the D_E data.

Furthermore, an approach to calibrate autoradiographic images for quantitative use is suggested. Using pressed powder pellets of reference materials, a series of calibration images were exposed, from which a functional relation between specific sample activity and greyscale value in the autoradiographic image has been deduced. Testing the calibration on a set of 16 geological samples, of which their radionuclide content is known, shows a good correlation between specific activities calculated from the nuclide content and specific activities deduced from the autoradiographic images. These findings illustrate the potential of autoradiography with imaging plates to detect spatial distributions of radionuclides and to tackle certain aspects of the problem of microdosimetry in modern trapped charge dating.

Keywords: imaging plate; autoradiography; microdosimetry; OSL; trapped charge dating; spatially resolved radioactivity.

1. INTRODUCTION

Over the last decades, trapped charge dating methods and their application to geological material have seen an extensive development and refinement. They are now a commonly used tool for dating samples ranging from Quaternary sediments to archaeological artefacts. In particular, the introduction of the single-aliquot regenerative dose (SAR) protocol by Murray and Wintle (2000) for Optically Stimulated Luminescence (OSL) dating, enables that all measurements to obtain equivalent dose

(D_E) estimates can be made on single aliquots or even single grains. This allows the determination of D_E distributions as inherent properties of a sample, based on the external variance of the SAR measurements. In recent years, it has become increasingly evident that broad D_E distributions can often be attributed not only to partial bleaching or experimental scattering, but also to the effects of microdosimetry (e.g. Vandenberghe *et al.*, 2003; Lomax *et al.*, 2007; Preusser *et al.*, 2007). The main cause for such small scale local heterogeneities in dose rate are spatially discrete high radiation emitters (e.g. K-rich feldspars, zircons or monazites) which form radiation "hot-spots". This is especially important in the case of alpha and beta radiation, which are not only the major

Corresponding author: D. Rufer
e-mail: rufer@geo.unibe.ch

contributors to luminescence dosimetry, but also exhibit far stronger spatial variations (due to their strong intensity falloff in particulate matter) than e.g. gamma radiation. While the widely used gamma-spectrometry allows to accurately determine dose rates differentiated by radionuclides, it is an integrated measurement method that yields no information about the spatial distribution of the sources of the measured radiation. Even though this problem is of concern to all trapped charge dating methods, its ramifications are more pronounced when using small aliquot sizes. This especially holds true for single grain OSL dating, as the overall percentage of grains in a sample which are in the vicinity of radiation hotspots and therefore subject to their localized high radiation fields is linked to the hotspot concentration. An increasing number of high radiation emitters therefore cause an increasing spread in incident radiation on individual grains in the sample. If the hotspot concentration gets very high, this effect abates due to increasing overlap of the localized radiation fields, resulting in higher but more homogeneous incident radiation for these grains. On the other hand, a very low hotspot concentrations leads to statistical insignificance of high incident radiation grains. It would therefore be desirable to have a method available to visualize such hot-spots or areas of elevated radionuclide concentration, in order to verify whether the assumption of applicability of the average infinity-matrix dose rate is valid for this sample, or whether an observed scatter in DE could also be attributable to non-uniformity in the spatial distribution of radionuclides.

In this article, we demonstrate the application of computed autoradiography using an imaging plate (IP) as a passive detection method to qualitatively document spatially resolved radioactivity in the context of trapped charge dating. The method constitutes a rapid screening and visualization procedure, which is applicable to various types of geological sample material and is non-destructive to the trapped charge signals. While an absolute calibration of the relationship between radiation energy and radiographic signal is still outstanding, we present a first investigation into using IP readout data for quantitative dosimetry.

2. THE PROBLEM OF DETERMINING NON-UNIFORM RADIATION FIELDS IN THE DOMAIN OF TRAPPED CHARGE DATING

Usually the possibility that microdosimetry might have an influence on measured D_E is perceived only "after the fact", i.e. by observing a large spread in D_E that cannot – or only partially – be explained by variations in luminescence sensitivity and dose saturation characteristics (Duller *et al.*, 2000), incomplete bleaching (Olley *et al.*, 1999), or post-depositional mixing (Bateman *et al.*, 2003). At that stage, determination of the nature, quantity and distribution of potential sample constituents that might have caused a heterogeneous radiation field can most often only be made on another part of that sample, as luminescence dating methods commonly require sample disaggregation and mineral separation for measurements.

This is acceptable for completely unconsolidated material, where the spatial arrangement of the different particles making up the sediment must – due to the inevitable perturbation during sampling and sample handling – be taken to be homogeneous on the scale of the sample volume. For such material, spatial dose rate distribution is a statistical property linked to the relative concentrations of the various particle types in the sediment and their respective dose rates. Monte Carlo models to describe and quantify the microdosimetric effects of non-uniform dose rate and dose rate distributions to single grains in heterogeneous sediments have been suggested by Nathan *et al.* (2003) (β radiation), Brennan (2006) (α radiation) and Mayya *et al.* (2006) (^{40}K grains in quartz matrix).

However, in the case of hardrock samples or meta-consolidated material like sediment drill cores, variations in radiation can be structurally caused (e.g. veining or sedimentary layering) and obtaining information about its original spatial distribution allows to select parts of the sample that are either not influenced by differential radiation or where the variability is at least more uniform. Therefore, such inquiries must be made on the same material that is going to be processed for and then measured by luminescence methods, unless the measurement method does not require sample dissagregation (e.g. spatially resolved luminescence measurements using CCD imagers (Greilich *et al.*, 2002; Greilich *et al.*, 2005)). Any other case requires that these preliminary analyses must be non detrimental to the quality of the natural luminescence signal and must keep the bulk structure of the sample intact. Moreover, they must also be feasible on larger samples, thus retaining the possibility for sufficient quartz or feldspar to be extracted (e.g. from parts of the sample that were selected due to radiation homogeneity). This forecloses most of the commonly used techniques for (radioactive) element mapping on solid samples like electron probe micro-analyzers (EPMA) or laser ablation inductively coupled plasma mass spectrometry (LA-ICP-MS) due to exposure of the sample to electromagnetic irradiation or light as well as due to stringent limitations in sample size. Optical microscopy could accommodate larger sample sizes, but lacks the required resolution and still poses the problem of requiring light.

3. COMPUTED AUTORADIOGRAPHY SYSTEMS

The basic constituents of an autoradiography system are: the sample material, which emits a radioactive signal; the image sensor, in this case the IP, which temporarily stores the energy pattern from the emitted radiation; the image reader (often colloquially called a "beta-scanner"), which reads out the latent image of the IP and converts it into an analogue and subsequently digital signal, and finally the image processor, which turns that signal into a greyscale image representing the spatial distribution of the signal produced on the imaging plate by the emitted radiation from the sample.

The sample material

Samples can consist of a wide range of materials and sample types (e.g. cut stones, sand, thinsections (Hare-

yama *et al.*, 1998), pressed powder pellets), with sample size only limited by the size of the IP. The sample must be dry and have a flat contact surface to the IP, both to produce a sharp autoradiographic image as well as to prevent scratching and uneven load on the IP (which is susceptible to moisture and mechanical damaging). Previous studies have demonstrated the cardinal applicability of IP autoradiography to crystalline rocks (Hareyama *et al.*, 1998; Hareyama *et al.*, 2000; Tsuchiya and Hareyama, 2001) and to speleothems (Cole *et al.*, 2003; Pickering et al., accepted manuscript).

The image sensor

Image plates are flexible, two-dimensional, integrating-type radiation sensors with a wide dynamic range in the order of five magnitudes. They consist of a backing foil coated with a layer of phosphor crystals embedded in an organic polymer binder, often sealed by a thin protective layer against humidity and mechanical wear. The photostimulable phosphor generally is barium fluorohalide activated with divalent europium ions ($BaFX:Eu^{2+}$, where X consists of Br and/or I, with modern IPs usually having a composition of $BaFBr_{0.85}I_{0.15}:Eu^{2+}$). A thorough disquisition on imaging plates and photostimulable phosphors is given in Rowlands (2002), Salis (2003), Schweizer (2001) and Spaeth (2001).

Autoradiographic exposure of an IP is achieved by placing the radioactive sample material directly onto the plate for a certain exposure time. The image plate absorbs radiation emitted from the sample, causing Eu^{2+} to oxidise to Eu^{3+} and the liberated electron can subsequently be trapped at a Br or F vacancy, introduced during the manufacturing process of the IP (Takahashi, 2002). This results in a density pattern of filled electron traps, corresponding to the distribution of radiation intensity emitted by the sample. As the fraction of electrons that can be trapped is linked to the availability of free traps, rising irradiation leads to decreasing trapping efficiency until all available traps are charged and the IP is saturated.

The image reader and image processor

During readout, the IP is longitudinally transported through the imager and laterally scanned by a fast-moving laser-beam in the red part of the spectrum (usually generated by solid state laser diodes [λ=680 nm] or continuous HeNe gas lasers [λ=633 nm]). This results in an excitation of the trapped electron and their relaxation to the ground state, thereby causing the emission of 390 nm blue light (in the case of $BaFBr_{0.85}I_{0.15}:Eu^{2+}$) in a pattern of parallel scan lines. The stimulated as well as the incident light are collected by a light guide, routed through a filter to block the red parts of the spectrum and then funnelled into a high-sensitivity photomultiplier tube. The recorded time-variant analogue signal is subsequently amplified, filtered to reduce signal noise and then digitized into a greyscale image (Miyahara, 1989; Rowlands, 2002) (**Fig. 1**).

As not all luminescence centres release their charge during the short dwell time of the excitation laser on one spot during a normal readout, multiple scans can be obtained from the same IP. The resulting images can then be stacked to increase signal/noise ratios

In order to reuse the image plate, any residual latent charge remaining on the IP after readout must be removed by bleaching the IP with a high intensity light source (usually high-pressure sodium or fluorescent lamps (Seibert, 1997) for several minutes.

4. METHODOLOGY

Samples and sample preparation

In this study, the following types of samples were used (see also **Table 1**):

- Unconsolidated samples: a glacifluvial sand from the Swiss alpine foreland (sample "LAW-2") and an aeolian dune sand from central Australia (sample "MS-8"). While the Swiss sample is an immature sediment with a very heterogeneous composition, the Australian sand consists almost exclusively of quartz with very few grains of predominantly feldspar and subordinate other minerals.

- Hardrock samples: a proterozoic pegmatitic basement rock from central Madagascar of predominantly granitoid composition (sample "DR076_3") and a 3 mm thick granite slab from the Aarmassiv, Switzerland (sample "GG_slab_b"). The presence of radioactive elements in accessory minerals like monazite, zircon and allanite leads to highly inhomogeneous microdosimetric conditions in these specimens.

- Pressed powder pellets of unconsolidated sample material: comprising both geological samples (where the radionuclide content has been independently established by gamma-spectrometry) as well as IAEA standard materials with known radionuclide concentrations, these specimens were used to investigate into possible absolute or relative quantification of the radiographic signal output.

Regardless of sample type, preparation of any material which will later on be used for luminescence measurements must be done without exposing the sample to light or heat. In the case of unconsolidated sample material (e.g. sand), the main interest lies in detecting a contingent radiation inhomogeneity and obtaining information about the relative amount of radiation hotspots as a statistical property of the sample as a whole. Therefore no preparation beyond drying of the sample was required and the material was simply sprinkled in a homogeneous layer of approximately 3 mm thickness onto the IP.

The hardrock samples had to be cut in order to obtain a flat surface for the autoradiography as well as for subsequent manual breaking and extraction of selected "target grains" to be measured for luminescence. Any cutting must be done under subdued red light, while taking utmost care not to generate heat or frictional sparking. Therefore the samples were mounted on a raisin bed and very slowly cut under cold water into slabs of 3 - 5 mm thickness. This allows the recording of autoradiographs on both sides of each slab.

The pressed powder pellets consist of a mixture of finely ground, homogenized sample material and an organic binder ("Fluxana BM-0002-1 Licowax"; $C_{38}H_{76}N_2O_2$; CAS-Nr. 00110-30-5), which is pressed into
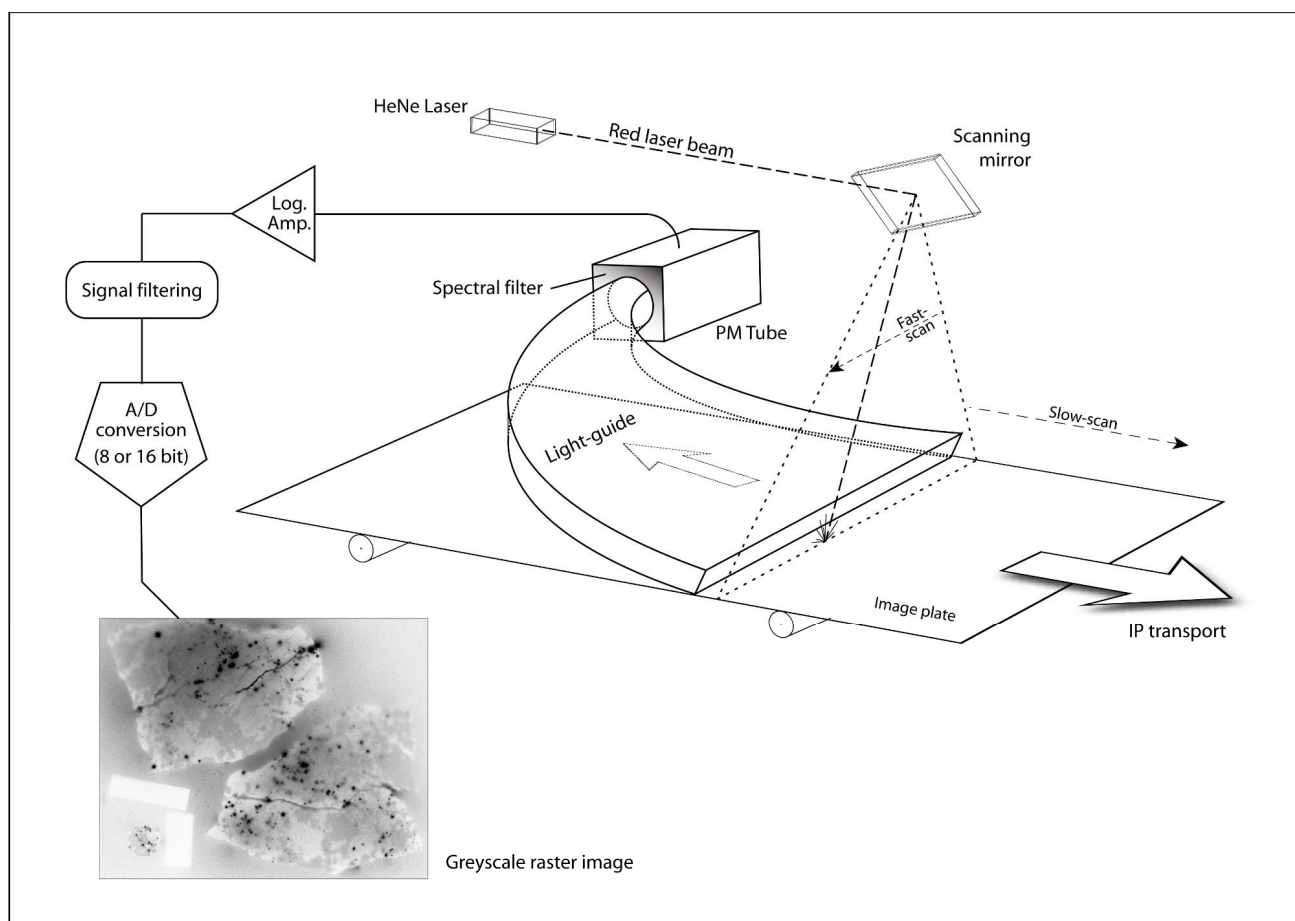
Fig. 1. *Schematic diagram illustrating the IP readout mechanism.*

a 3.2 cm diameter disc with a hydraulic hand-press at 300 kg cm^{-2}. Blank tests have shown no signal contribution from the binder to the radiographic image and the binder / sample ratio can be chosen to accommodate enough binder to create a cohesive pill after pressing, with coarser sample material commonly requiring higher ratios. Unlike their unconsolidated source material, the pressed pellets can be used for multiple measurements without any changes in the sample geometry and composition during handling. Their size permits up to 30 pellets to be placed on an imaging plate at one time without risking irradiation from one pellet influencing the radiographic images of neighbouring pellets.

For the geological samples in this study, a weight-ratio of 2:1 with a resulting total weight of 3.00 g for the mixture was used, as this proved to be a good compromise between pill quality and not diluting the sample material overmuch. The average pellet thickness of 2.32±0.05 mm and average pellet density of 1.59±0.04 g cm^{-3} allow the geometry and the β-attenuation within the geological sample pellets to be considered as similar (**Table 1**).

For the calibration pellets, a self-made mixture of IAEA reference materials RGK-1 and RGTh-1 (IAEA Report RL 148, 1987) was used with a ratio of 36 / 19 respectively. This mixture was then added to the organic binder to create a series of 3.00 g pellets with varying radionuclide concentrations. The calibration pellets have

an average thickness of 3.69±0.03 mm and an average density of 0.99±0.01 g cm^{-3} (**Table 1**). The discrepancy between the sample and calibration pellets in terms of average thickness and density is due to the pellet pressing mechanism. As the mould did not allow constriction to a certain pellet height, all pellets were pressed at the same pressure, resulting in systematically lower densities for the calibration pellets which contain a far higher percentage of the low density organic binder.

Exposure, readout and image treatment

In order to allow a comparison, all exposures of the IPs were done in a temperature controlled basement lab at 21°C inside a 5 cm thick radionuclide-free lead-box, with an additional internal shielding of 1 cm of wood and 1 mm of copper in order to minimise the effects of secondary X-rays generated by particle – matter interactions in the lead shielding.

In this study we used the commercially available 23 × 25 cm BAS-MS IP from Fuji Photo Film Co Ltd. A 9 μm thick protective layer out of Mylar makes it sufficiently robust for use even with geological samples. The phosphor layer has a thickness of 115 μm with the individual phosphor crystals typically having a grain size of 4-5 μm (Matsuda *et al.*, 1993).

The image reader used is a BAS-1800 Bio-imaging Analyzer System from Fujifilm Life Science Corporation,

Table 1. *Samples used in this study with their respective radioactivity (given as decays per minute (dpm) for the sample mass), radionuclide concentration and the geometry of the sample pellet.*

	Sample name	Sample description	Activity (dpm)	K (wt%)	Th (µg g⁻¹)	U (µg g⁻¹)	Pellet thickness (mm)	Pellet density (g cm⁻³)
Standard material for quantitative analysis	CS-0.4	calibration pressed pellet	12.98±0.11	0.21±0.001	2.04±0.13	0.02±0.0004	3.71	0.98
	CS-0.7	calibration pressed pellet	22.82±0.19	0.37±0.003	3.59±0.23	0.03±0.0006	3.71	0.98
	CS-1.0	calibration pressed pellet	32.76±0.28	0.53±0.004	5.12±0.33	0.04±0.0008	3.71	0.98
	CS-1.3	calibration pressed pellet	42.87±0.36	0.70±0.005	6.70±0.43	0.05±0.0010	3.69	0.99
	CS-1.7	calibration pressed pellet	55.82±0.47	0.91±0.006	8.74±0.55	0.07±0.0014	3.71	0.98
	CS-2.0	calibration pressed pellet	65.31±0.55	1.07±0.007	10.27±0.65	0.08±0.0016	3.70	0.98
	CS-2.5	calibration pressed pellet	81.96±0.69	1.33±0.009	12.81±0.81	0.10±0.0020	3.68	0.99
	CS-3.0	calibration pressed pellet	98.13±0.83	1.60±0.011	15.41±0.98	0.12±0.0024	3.61	1.01
	RGU-1 Pill	pure, for shielding-test only	n.d.	< 20 µg/g	< 1	400±2	--	--
	RGK-1 Pill	pure, for shielding-test only	n.d.	44.8±0.3	< 0.001	< 0.01	--	--
Geological sample pellets for quantitative analysis	Gemmi 1	loess, Switzerland	33.30±1.07	0.48±0.01	3.82±0.26	1.81±0.07	2.40	1.54
	Gemmi 2	loess, Switzerland	31.51±0.70	0.45±0.01	3.94±0.23	1.83±0.07	2.42	1.52
	P 32	fluvial sediment, Slovenia	60.60±0.87	0.94±0.01	4.74±0.35	1.72±0.10	2.36	1.60
	P 33	fluvial sediment, Slovenia	18.12±0.61	0.27±0.01	1.19±0.01	1.14±0.10	2.24	1.65
	MSK 1	fluvial sediment, Slovenia	79.21±1.57	1.23±0.01	9.93±0.58	2.05±0.18	2.33	1.58
	MSK 2	fluvial sediment, Slovenia	78.16±1.24	1.21±0.01	10.00±0.51	2.36±0.23	2.36	1.55
	Ill 1	alluvial deposit, Switzerland	97.83±2.10	1.69±0.02	3.09±0.28	1.25±0.35	2.28	1.61
	POSL 2	aeolian sand, Peru	63.92±1.57	1.07±0.01	4.30±0.27	1.03±0.28	2.36	1.56
	POSL 11	aeolian sand, Peru	64.41±1.14	1.02±0.01	4.51±0.27	2.29±0.25	2.28	1.61
	MaJ 4	fluvial sediment, Peru	71.53±1.58	1.21±0.01	4.48±0.15	0.72±0.32	2.24	1.65
	MaJ 8	fluvial sediment, Peru	72.39±1.56	1.21±0.01	5.90±0.12	0.83±0.32	2.28	1.62
	MaJ 9	fluvial sediment, Peru	84.52±3.81	1.37±0.01	7.00±0.11	1.75±1.30	2.36	1.56
	MaJ 10	fluvial sediment, Peru	90.88±2.29	1.51±0.01	6.19±0.05	1.52±0.66	2.30	1.61
	MaJ 14	fluvial sediment, Peru	95.99±2.04	1.56±0.01	7.19±0.31	2.17±0.47	2.31	1.60
	MaJ 16	fluvial sediment, Peru	92.09±1.73	1.53±0.01	6.25±0.28	1.53±0.35	2.30	1.60
	RAT 3	fluvial sediments, Slovenia	77.55±1.31	1.28±0.01	5.32±0.40	1.54±0.13	2.30	1.60
Hardrock samples	DR 076_3	Pegmatite	n.d. (qualitative analysis only)					
	GG_slab_(b)	Granite slab, Grimsel, Switzerland	n.d. (qualitative analysis only)					
Sand samples	LAW-2	glacifluvial sediment, Switzerland		1.09±0.04	4.10±0.03	0.97±0.03		
	MS-8	aeolian sand, Australia	21.7	0.54	2.35	0.53		

which has an imaging capability with a minimal pixel size of 50 μm and a dynamic range of approximately five orders of magnitude.

Removal of the samples from the IP and transfer of the latter into the image reader was done under strongly subdued red light, as not to impair the recorded signal. In order to have procedural consistency, the first scan was taken exactly one minute after the end of exposure and removal of the samples, each subsequent scan of the same IP was then taken in immediate succession, up to three stacked scans. The internal reproducibility of the measurement protocol has a standard deviation of 0.4%, established on five repetitive measurements of five samples.

For imaging and qualitative analysis, the sample is placed directly on the IP in order to achieve maximum sharpness, similar to the effect of a photographic contact copy. Autoradiographs of the pressed powder pellets (or any other sample on which the signal is to be used in a quantitative manner) are obtained with a 0.3 mm thick shield of paper ($0.8 \, g \, cm^{-3}$) between samples and IP, acting as an α-particle absorber.

For a qualitative application, it can be beneficial to trim the full greyscale spectrum to the signal latitude recorded from the sample, in order to increase signal to noise ratios. Increasing image contrast curves can also aid illustrative purposes (**Fig. 2**), as can inverting the greyscale values.

However, in the case of an intended quantitative use, any image treatment applied to radiographic images must preserve the original signal linearity of the image. This requires that greyscale values from trimmed spectra must be recalculated to the full spectral width in order to enable a comparison with the measurements from other images. Also, any contrast enhancement done with non-linear input / output curves introduces differential gradation over the remaining spectrum, rendering quantification impossible.

PSL signal production from different types of radiation

While the radiation intensity distribution of a sample is inherently a 3-dimensional property, self-shielding within the sample material and defocusing of radiation contrasts with increasing distance between the emitter and the IP / sample contact surface leads to the recorded image being dominated by the radiation pattern from a layer close to the sample's contact surface. The thickness of this layer is dependant on the material properties of the sample and the type and energy of the radiation in question. Considering the orders of magnitude of effective ranges of U, Th and K derived α-, β- and γ-rays in quartz as exemplifying values for such radiation ranges in crustal rocks and terrestrial sediments – which make up
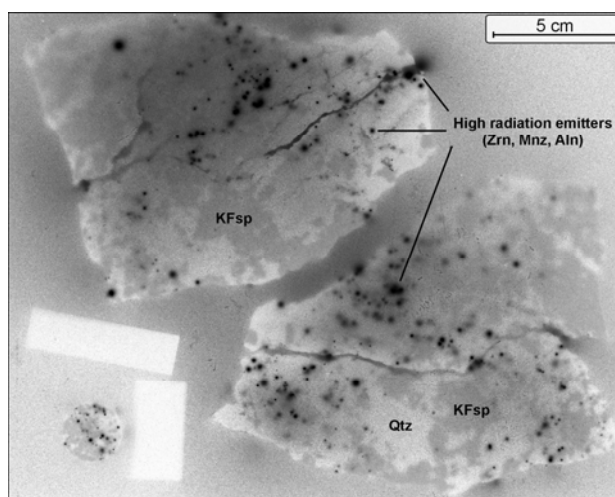

Fig. 2. *Autoradiography of pegmatite sample "DR076_3". Clearly distinguishable are high radiation sources like zircons, monazites or allanites (black hotspots), less radiation emitting K-feldspars (grey) and radiologically inert quartz. The white rectangles are due to PVC shielding blocks and the round sample is an orthogneiss with similar petrography.*

most of the commonly used sample types – the maximum thickness of this contributing layer lies in the range of $< 35 \, \mu m \, (\alpha)$, $< 2 \, mm \, (\beta)$ and tens of cm (γ).

As any radiation emitted by the sample must also pass the 9 μm Mylar layer of the IP, the thickness of the contributing layer lying in the sample itself (and thus actually containing radionuclides) is only 25 μm or less for α radiation. Due to this and the strong intensity falloff of α radiation in matter, the majority of α particles contributing to the autoradiographic image will originate from only a very small fraction of the sample volume close to the contact surface. Based on the same principle, the effect of a sample's γ emission on the autoradiograph will be rather homogeneous due to its highly penetrative nature, thus simply adding to a uniform base signal in the IP. If a background deduction is made to correct for any signal produced by cosmic radiation, the γ derived uniform signal portion – which extends well beyond the actual sample surface – is also for the largest part being subtracted. As a consequence, with the number of α emitters being subordinate due to a small source volume and γ emission being largely subtracted, β radiation is considered to be the main contributor to the differential signal intensities of the radiographic image. This is corroborated by a shielding experiment, in which a comparative time-series of autoradiographs of two homogenized radiation sources ("RGU-1 Pill" and "RGK-1 Pill", see **Table 1**) were successively exposed with various amounts of shielding between source and IP (**Table 2**).

Table 2. V_{PSL} generated by identical source material with differing amounts of shielding.

Exposure time (h)	no shielding		0.3 mm paper ($0.8 \, cm^{-3}$)		4 mm Al ($2.66 \, g \, cm^{-3}$)	
	RGU-1 Pill	RGK-1 Pill	RGU-1 Pill	RGK-1 Pill	RGU-1 Pill	RGK-1 Pill
52	10240	9187	8762	7940	1345	319
76	11233	10240	9837	8899	1883	517
124	12327	11357	11040	10082	2720	613

After adding 0.3 mm of paper (ρ=0.8 g cm^{-3}), a small reduction in PSL signal of around 14% was observed, which is attributed to the complete shielding of the remaining α-particles that previously reached the IP. Subsequently, using 4 mm of aluminium shielding (ρ=2.66 g cm^{-3}) in order to block all β-radiation resulted in a far stronger reduction of the PSL signal of 83% ("RGU-1 Pill") and 95% ("RGK-1 Pill").

5. QUALITATIVE DETERMINATION OF RADIATION INHOMOGENEITY

An example of an autoradiograph of a pegmatitic hardrock specimen (sample "DR076_3") is given in **Fig. 2**. There is a clear distinction between the grey rendering of the K-feldspars and the lighter, non radiogenic quartz and plagioclase grains, which show no signal above background. Notable is also the highly heterogeneous distribution of small high-radiation emitters which form black hotspots on the image. Usually these are accessory minerals such as zircons, monazites or allanites, which contain high concentrations of U and Th. Their strong radiation emission even causes "bleeding" of their image due to volume effects upon interaction with the imaging phosphor. This can be seen along the right edge of the upper sample, where a radiation halo causes exposure to radially extend beyond the sample edge.

Fig. 3 shows a comparison between the autoradiograph of a deformed granite slab (Sample "GG_slab_(b)") and the corresponding optical image of the sample surface. The areas of high signal intensity (with the exception of the hotspots) correspond to the location of larger alkali feldspar grains, and Hareyama *et al.* (1998) and Tsuchiya and Hareyama (2001) have shown a basic relationship between increasing K$_2$O content and increasing PSL signal. The hotspot locations in the autoradiograph cannot be traced to any visible mineral phase in the optical image. This indicates that the constituents causing these radiation inhomogeneities cannot be identified by mere optical observation, especially when the sample must not be subjected to light microscopy.

Concerning unconsolidated samples, **Fig. 4** shows a juxtaposition of autoradiographs from two very different sedimentary materials. Sample "LAW-2" (**Fig. 4a**) is an alpine, proglacial sediment derived from a geologically complex source region comprising molasse, limestones and granitic crystalline rocks (which are akin to sample "GG_slab_(b)"). Its sedimentary history is characterized by short transport distances, little sedimentary reworking and minor chemical weathering. This is reflected in the autoradiograph by an increased overall signal level (most of the K-feldspar is still intact), and an inhomogeneous radiation pattern with a significant number of radiation hotspots, indicating that the heavy minerals have not yet been lost to mineral partitioning during transport and sedimentation. It is therefore a representative example of an autoradiograph from a rather immature sediment of very heterogeneous petrographical composition. Such an image gives an indication, that microdosimetry may be a
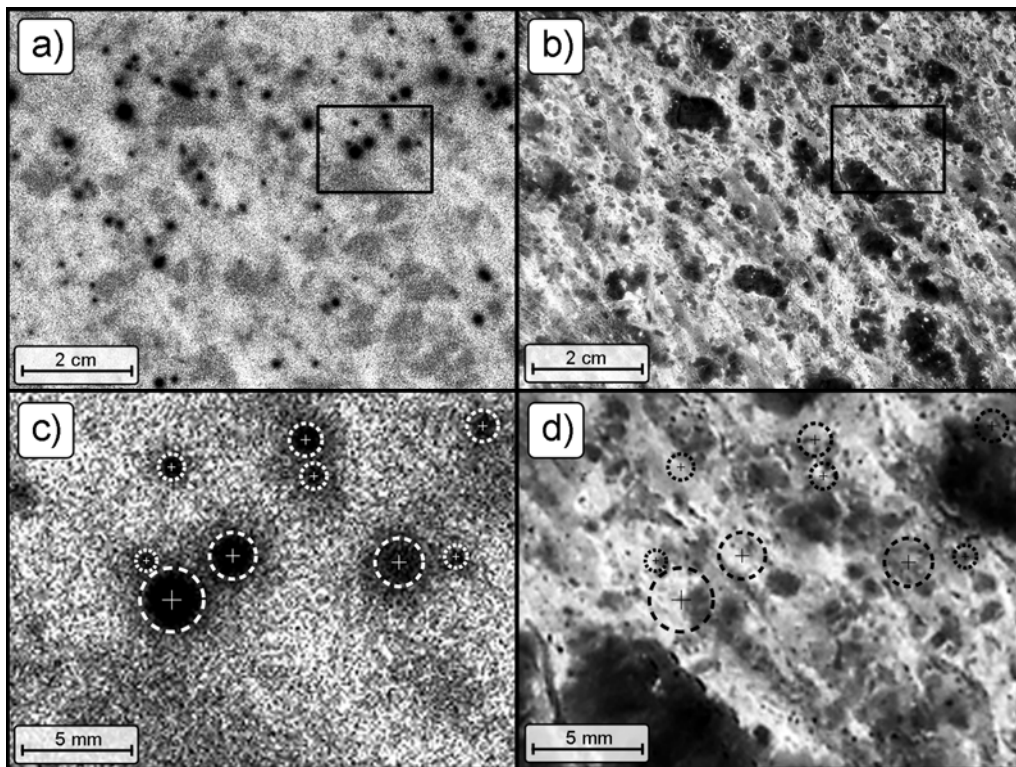

Fig. 3. *Comparison of autoradiography and optical image of a granite slab (sample "GG_slab_(b)"): a) radiographic image showing the distribution and intensity of the photostimulated luminescence; b) optical scanning image of the polished slab surface (inverted greyscale image, dark areas are K-feldspar grains). Framing is identical for both images and the rectangle indicates the section depicted in the close-up images below. c) and d): while the locations of the K-feldspar grains can be traced in the radiography, the sources for the hotspots are not identifiable in the optical image at this magnification.*

factor to be considered when interpreting OSL data from such a material.

Sample "MS-8" (**Fig. 4b**) is an aeolian dune sand from central Australia, representing a very matured sample that experienced important chemical weathering and a long sedimentary history with repeated phases of reworking, (aeolian) transport and redeposition. With quartz being the dominant mineral constituent and only a negligible amount of feldspar and heavy minerals, the corresponding autoradiograph shows a homogeneous radiation distribution with no discernible hotspots. The overall low radioactivity of this sample necessitated an increase in exposure time in order to record sufficient signal.

While aeolian dune sands from this region are generally assumed to be well bleached, broad D_E distributions have been reported by Lomax *et al.* (2003; 2007) for numerous other samples. Without excluding the possibility of post-depositional mixing, microdosimetry is also taken into consideration and Lomax *et al.* (2007) indicate that either high radiation sources like zircons or differential shielding of quartz grains due to carbonate or iron-oxide coating might cause the observed D_E overdispersion. In the case of sample "MS-8", autoradiography allows to exclude the presence of high radiation emitters such as zircons as a likely cause for microdosimetry and therefore provides an important information when interpreting the OSL data.

It can be seen that such qualitative screening therefore efficiently gives precursory information whether a sample has to be considered to be variable with regards to dosimetry or not. If, based on these findings, the sample is considered homogeneous in terms of radiation or is discarded altogether, such a qualitative inquiry may suffice. On the other hand, the availability of spatially resolved, relative radiation information evokes a demand for a means of absolute calibration of the information inherent in such images. An established calibration would then allow to just as rapidly obtain absolute dosimetric values.

6. FIRST INVESTIGATIONS INTO THE POTENTIAL TO QUANTIFY PSL SIGNALS

As pointed out in the previous section, it would be desirable to have a method available to quantitatively evaluate entire samples or regions of interest in a radiographic image in order to deduce spatially resolved dose rates. To do so, it is necessary to develop a mathematical relationship between the dose emitted from the sample and the signal recorded from the IP in such a region of interest. The complexity and the multitude of physical and chemical factors involved in the production and the reading out of this signal makes a backward calculation model infeasible. We therefore investigate into the potential of experimentally calibrating the signal output by means of calibration standard materials.

While PSL stands for the process of photostimulated luminescence and for the latent image stored in the IP as a non-quantitative entity, the term "PSL-value" has been defined by Mori and Hamaoka (1994) as the "detected photostimulated luminescence value under certain standard conditions of the designated kind of X-ray, radiation amount [and] timing of reading after exposure". As this is therefore simply a question of normalization factor, we use the term "PSL-value" (V_{PSL}) in this paper as the background corrected, averaged greyscale value of a certain area of the resulting image.

Theoretical background

Using exposures of one hour, a positive linear relation between PSL signal [given as a.u. mm^{-2}] and specific activity A [given as dpm mm^{-2} per unit mass] was described first by Amemiya and Miyahara (1988) to be a fundamental property of IPs. This relation was found to be different for various radionuclides, giving specific linear factors k_i for different nuclides i and their respective radiation spectrums:
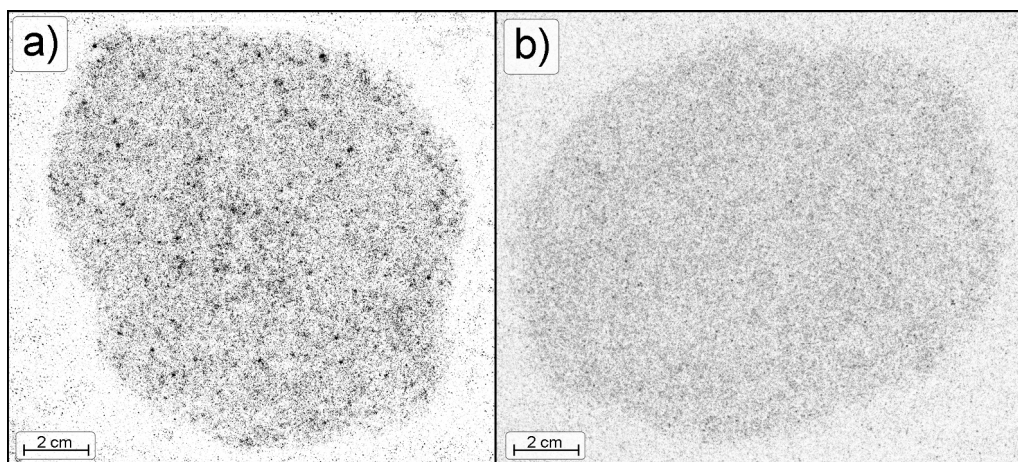

Fig. 4. *Autoradiographs of unconsolidated sand samples. The sand was poured onto the IP and then spread with a spatula by hand to a thickness of 2 – 3 mm. A 12 µm cellophane layer was put between the sample and the IP to facilitate sample removal. a) glacifluvial sample "LAW-2"; b) aeolian dune sand sample "MS-8". Exposure times were 70.5 h ("LAW-2") and 112 h ("MS-8") in order to accumulate enough signal in the autoradiograph of the low activity sample "MS-8".*

$$V_{PSL_i} = k_i A_i \qquad (6.1)$$

V_{PSL_i} V_{PLS_i} also correlates positively with exposure time t, albeit not in linear fashion. As the specific activity A_i can be considered to remain constant over the time range of measurement, *(1)* can be extended to:

$$V_{PSL_i}(t) = k_i(t) A_i$$

which can be rewritten as:

$$V_{PSL_i} A_i^{-1}(t) = k_i(t) \qquad (6.2)$$

Thus, if $k_i(t)$ can be formulated (e.g. by regression of a k_i vs. t plot), the specific activity A_i can theoretically be calculated from the V_{PSL_i} of an autoradiograph and its exposure time t.

In the literature, such linear relationship are only described for mono-nuclide radiation (e.g. Amemiya and Miyahara, 1988; Mori and Hamaoka, 1994; Gonzalez *et al.*, 2002) and not for decay chains. In the latter cases – if secular equilibrium is assumed – the resulting linear relationship would be a weighted composite of all the linear relations of the respective nuclides making up the decay chain. Extrapolating, the same concept can be applied to a bulk composition of radionuclides that make up a sample, using a theoretical nuclide as a representative for the entire sample's relative radionuclide composition (note: samples with varying *total* but identical *relative* radionuclide concentrations are therefore represented by the same theoretical nuclide, simply with varying concentration). In this case, the index i denominates the sample composition instead of merely a single radionuclide species and

the given formulations can be applied to describe the V_{PSL} generation of a sample with specific activity A as a whole.

Establishing a calibration curve

A sequence of autoradiographs with varying exposure times was taken from the entire set of calibration pellets in order to get a series of PSL-values variable in exposure time and total activity (**Fig. 5a**). As the calibration pellets contain increasing amounts of the same relative mixture of radionuclides, they emit the same radiation spectra. According to **Eq. 6.1**, the same linear relationship $V_{PSL}(A)$ should apply to all of them. Plotting V_{PSL} against A should therefore result in a set of straight lines going through the origin, with their slopes k given by the varying exposure times as described by **Eq. 6.2**. **Fig. 5b** however shows, that there is an increasing deviation from the postulated linearity of $V_{PSL}(A)$ for longer exposure times, which is attributed to saturation effects. As higher specific activities produce more signal in a given amount of time, they will also cause the IP to reach saturation faster. Therefore, **Eq. 6.1** becomes less valid with the resulting V_{PSL} approaching higher values and the term $k(t)$ in **Eq. 6.2** becomes increasingly influenced by A. This is illustrated in **Fig. 6**, which is a graphical representation of **Eq. 6.2** for three calibration pellets of low, medium and high activity. In the case of our calibration material, the divergence in signal production behaviour due to different specific activities becomes increasingly significant for exposure times above a threshold value of approximately 50 h. A saturating exponential model curve fitted to the
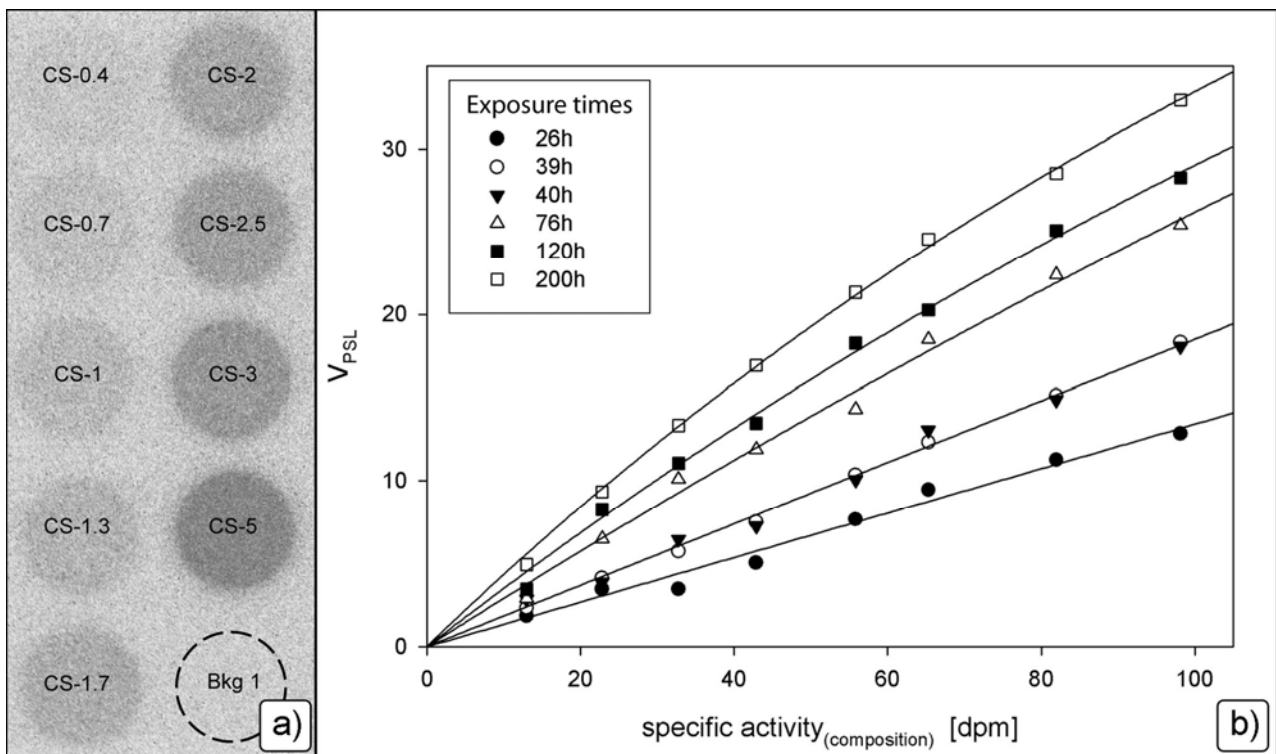

Fig. 5. *a) Stacked image from the 76h exposure showing the increasing PSL densities recorded on the IP with increasing radionuclide concentration in the calibration pellets (contrast enhanced for visualisation). "Bkg 1" indicates a background measurement. b) Correlations between specific activities (based on radionuclide content) and PSL-value for various exposure times.*

mean k values of the exposures below that threshold was therefore taken as the functional relation describing $k(t)$ for our calibration material (**Fig. 6** inset):

$$k(t) = 0.3484\,(1 - e^{-0.0185\,t}) \qquad (6.3)$$

In accordance with **Eq. 6.2**, it is therefore possible to calculate the specific activity of a sample based on the recorded V_{PSL} for a known exposure time.

To test the tolerance of the calibration, specific activities of the entire set of calibration pellets over a wide range of exposure times were calculated using **Eq. 6.3**. Comparing these to the specific activities from the radionuclide compositions gives an indication about how reliable the calibration works over a comprehensive range of parameters (**Fig. 7**). On the low signal side, low exposure time combined with low activities results in considerable scatter, due to bad counting statistics on the resulting low V_{PSL} (**Fig. 7a**). Meanwhile, for very long exposures, the varying saturation behaviour for different specific activities becomes apparent (**Fig. 7d**). However, exposures of 40 h and 76 h (**Fig. 7b** and **c**) both seem to indicate a range in exposure time in which the calibration seems to work fairly well and the calculated specific activities ratios of all calibration pellets lie within ±10% around unity. Care should therefore be taken to assure that the actual measurement procedure applied to the sample is identical to the procedure used when establishing the calibration, and that sample exposures be kept in the range of 40-76 h.

Application to geological samples

The applicability of the method to natural material was tested by applying it to a 50 h exposure, taken from the pressed pellets series of geological samples (**Table 1**). **Fig. 8** shows the correlation between their specific activities based on the nuclide content ($A_{comp.}$) and the specific activities calculated from the PSL-values (A_{PSL}), using **Eq. 6.3**. With exception of the far outlying values of the samples "Gemmi 1" and "Gemmi 2", the A_{PSL} / $A_{comp.}$ ratios of the geological material plot slightly above unity (mean = 1.12) with a standard deviation of 0.13.

Two aspects must be considered when interpreting these results:
1) The slight overemphasis of the A_{PSL} values of the geological material compared to the calibration pellets is seemingly of a systematic nature.
2) The observed spread in the samples is larger than in the calibration pellets. This indicates variations in the A_{PSL} of the geological material which seem to exceed the methods intrinsic variability, given by the spread of the calibration pellets (**Fig. 7**).

The first point is most likely related to the systematic difference in thickness and density between calibration pellets and geological pellets. As they are thinner, the radionuclide concentration close to the IP is higher in the sample pellets compared to the thicker calibration pellets. This appears to be only partly compensated by their higher density and hence higher internal attenuation of the emitted radiation.
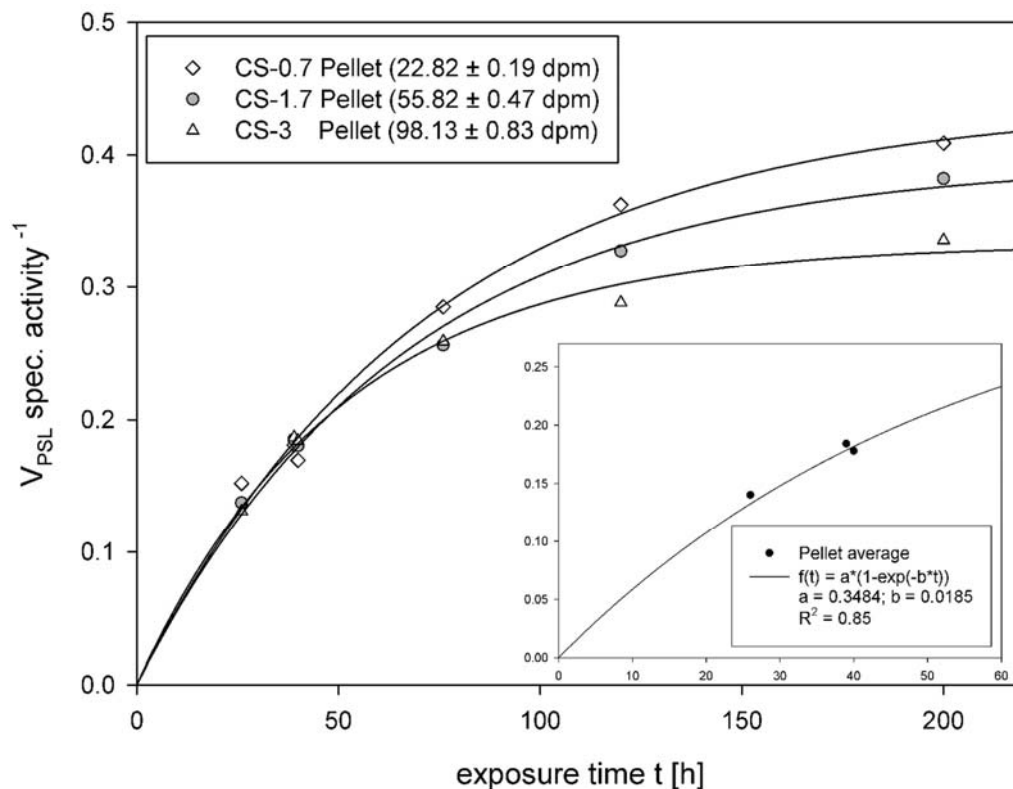

Fig. 6. *Increase of the regression line slopes from Figure 5b over time, plotted for a calibration pellet of low, medium and high specific activity. The fitting lines are saturating exponentials, illustrating the influence of specific activity on the saturation behaviour. Inset: saturating exponential curve fit through the calibration pellets mean values. This curve is used as the calibration curve.*

As to the second point, it has already been discussed that in order to compare two samples quantitatively, the same formulations of **Eq. 6.1** and **Eq. 6.2** must apply to both of them. This implies that an absolute calibration could only be made for samples with identical relative radionuclide composition as the calibration material. Comparing the results (**Fig. 8**) with the pellet compositions (**Table 1**), it can be seen that the two outliers "Gemmi 1" and "Gemmi 2" indeed show the lowest K / (Th + U) ratios of the geological material. **Fig. 9** plots the samples A_{PSL} / $A_{comp.}$ ratios against the fractions of

their specific activity originating from Th + U (X_{Th+U}, with $X_{Th+U} + X_K = 1$). This corroborates the influence of increasing relative Th and U concentrations on an overestimation of A_{PSL}.

A possible explanation for this observation could be that U emits multiple β-quanta throughout its decay chain which possess lower average energies than the β-quanta emitted by ^{40}K.

Tanaka *et al.* (2005) and Chen *et al.* (2008) have shown that PSL generation per electron increases no-
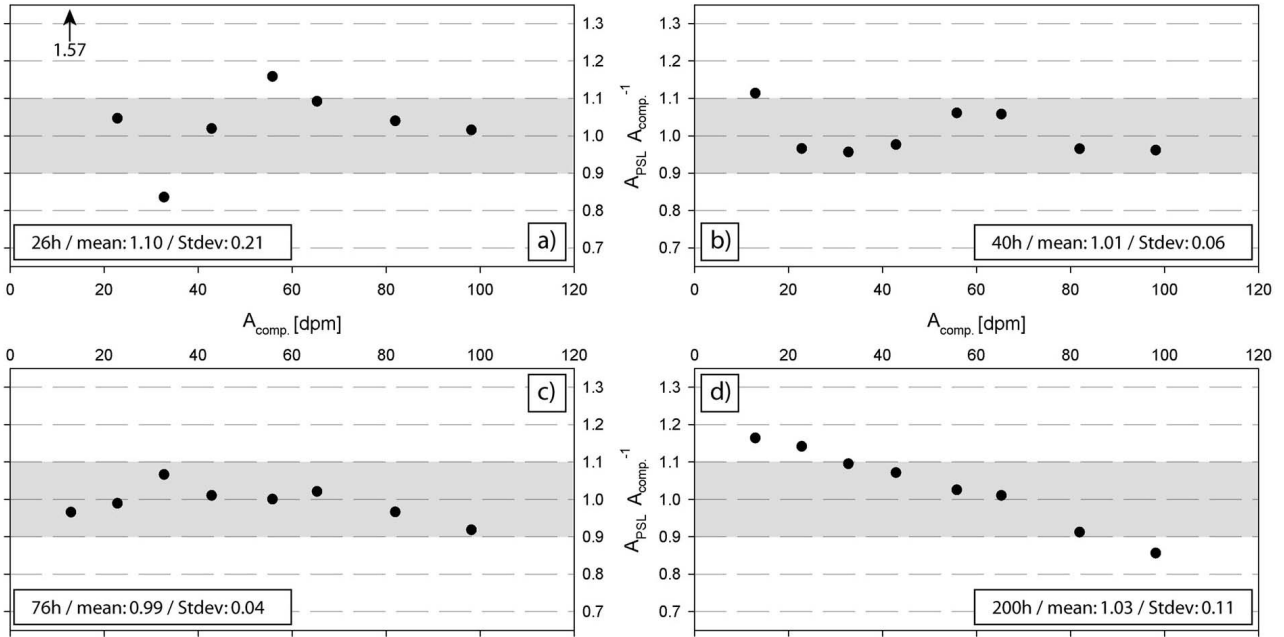

Fig. 7. *Comparison of A_{PSL} / $A_{comp.}$ ratios over the entire range of calibration pellet activities for different exposure times.*
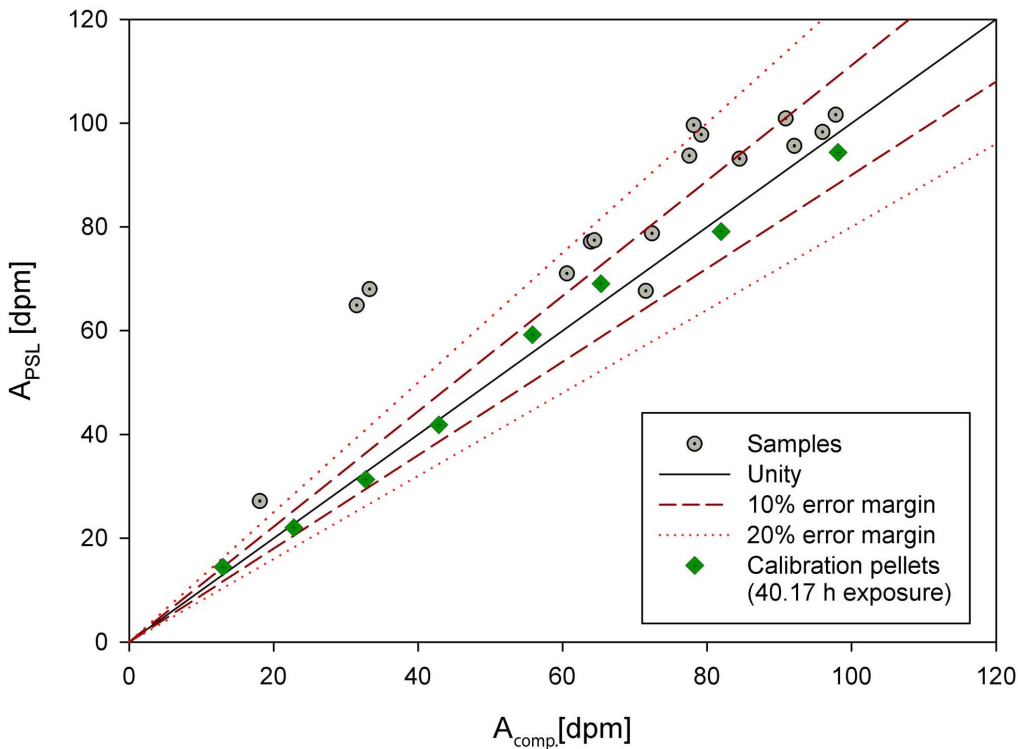

Fig. 8. *Juxtaposition of specific activities calculated from radionuclide content ($A_{comp.}$) and activities calculated from PSL-values (A_{PSL}) for the geological sample pellets. Exposure times were 50 h for the geological samples and 40.17 h for the calibration pellets given to illustrate the spread inherent to the method.*
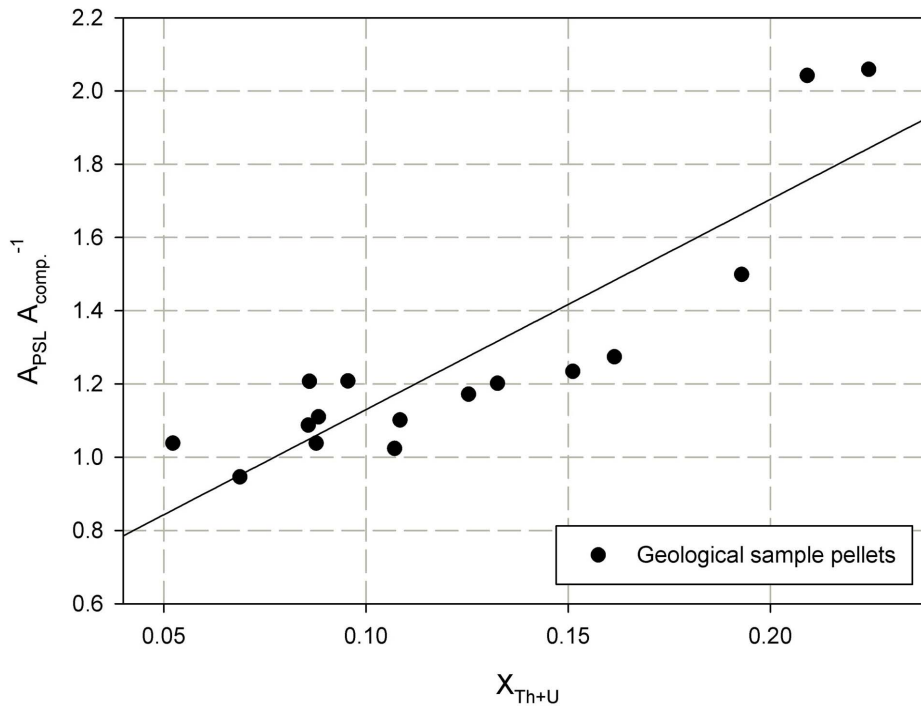
Fig. 9. *A positive correlation between growing relative content in Th + U and excessive A_{PSL} / $A_{comp.}$ ratios illustrates the influence of deviating relative radionuclide compositions for the applicability of the calibration. The abscissa is given as the Th+U fraction of the total U, Th and K content of the samples, with $X_{Th+U} + X_K = 1$).*

ticeably with decreasing electron energy below 1 MeV, an effect which is attributed to lower energy electrons generating more PSL-signal closer to the IP surface (Thoms, 1996). This in turn leads to a higher signal yield during readout and a relative overestimation of A_{PSL}.

While this demonstrates the need to reconcile radionuclide composition between samples and calibration material, the overall good correlation indicates that the calibration method is fairly tolerant towards this aspect.

The problem of linking specific activity and dose rates based on PSL-values

In the case of a single, known type of radionuclide and therefore a single, known radiation energy spectrum, the specific activity A is proportional to the emitted dose rate D and $V_{PSL}(A) \approx V_{PSL}(D)$. As β radiation is the principal contributor to the PSL signal, $V_{PSL}(D)$ is strongly influenced by the IPs signal production efficiency per electron (PSL / electron). Two countervailing effects play a role in this: a) below 1MeV, PSL / electron shows strong variations with electron energy up to a factor of four (Tanaka *et al.*, 2005; Chen *et al.*, 2008), and b) natural β radiation is not discrete, but forms a continuous spectrum over a certain energy range, depending on radionuclide. While the second effect dampens PSL variations introduced by the first effect, equal doses emitted by different radionuclides often still produce differing PSL values. In the case of a mixture of radionuclide species, the resulting β energy spectrum is the integration of the various species' spectra. The more different radionuclides such mixtures incorporate (especially when secular equilibrium is reached), the broader their resulting β spectrum becomes, leading to a decrease in the variation of $V_{PSL}(D)$ between such mixtures. Regardless of that, systematic tests using calibration sequences with fixed dose rates and variable radionuclide compositions would be re-

quired in order to establish a quantitative link between dosimetry and PSL-signal.

7. CONCLUSIONS

Autoradiography with imaging plates enables the spatially resolved detection and visualisation of radiation inhomogeneities in a wide range of sample types without being destructive to luminescence signals. It is a tool to rapidly assess relative β radiation levels within and between samples, and to provide information about the homogeneity of a given material's radiation field. The procedure does not require elaborate sample processing and provides the results in a graphical manner, which is well suited for interpretation.

Qualitative application of the method to consolidated or hard rock material allows visualization of high radiation areas or layers in a sample. In unconsolidated sediments, the detection of radiation inhomogeneities and hotspots provides important information about whether microdosimetry is to be expected as a likely contributor to a D_E overdispersion.

Information about spatial variability of radiation is essential for any kind of trapped charge dating, especially on material where microdosimetry must be considered a potential problem.

It allows for a better constraint of this important parameter, which is too often not properly taken into consideration because it can not be determined with the established method of dosimetry measurement (i.e. gamma-spectrometry). As such, imaging plate autoradiography of geological materials has its potential application not only in the context of luminescence dating. In the emerging field of speleothem dating by U-Pb and U-Th series, identifying layers of high radionuclide content is indispensable for successful dating (Cole *et al.*, 2003; Pickering et al., accepted manuscript). Similarly, Electron

Spin Resonance (ESR) dating of tooth enamel might profit from a rapid visualisation technique to determine relative radionuclide concentrations in the different tooth components.

A foray into quantitative calibration of the imaging plate is also presented, examining the potential of calculating a samples activity from the greyscale value of the recorded radiographic image. While certain limitations are identified and discussed, verification of the method using 16 geological samples of known specific activities illustrates its general applicability to geological materials. However, to obtain an absolute dosimetric calibration, further research is needed in order to link PSL generation not only to a sample's activity but to its emitted radiation energy. This would eventually enable determining dose rates from an autoradiograph, allowing to calculate spatially resolved D_E or quantify a microdosimetry derived D_E overdispersion.

REFERENCES

Amemiya Y and Miyahara J, 1988. Imaging Plate illuminates many fields. *Nature* 336(6194): 89-90.

Bateman MD, Frederick CD, Jaiswal MK and Singhvi AK, 2003. Investigations into the potential effects of pedoturbation on luminescence dating. *Quaternary Science Reviews* 22(10-13): 1169-1176.

Brennan BJ, 2006. Variation of the alpha dose rate to grains in heterogeneous sediments. *Radiation Measurements* 41(7-8): 1026-1031.

Chen H, Back NL, Bartal T, Beg FN, Eder DC, Link AJ, MacPhee AG, Ping Y, Song PM, Throop A and Van Woerkom L, 2008. Absolute calibration of image plates for electrons at energy between 100 keV and 4 MeV. *Review of Scientific Instruments* 79(3).

Cole JM, Nienstedt J, Spataro G, Rasbury ET, Lanzirotti A, Celestian AJ, Nilsson M and Hanson GN, 2003. Phosphor imaging as a tool for in situ mapping of ppm levels of uranium and thorium in rocks and minerals. *Chemical Geology* 193(1-2): 127-136.

Duller GAT, Botter-Jensen L and Murray AS, 2000. Optical dating of single sand-sized grains of quartz: sources of variability. *Radiation Measurements* 32(5-6): 453-457.

Gonzalez AL, Li H, Mitch M, Tolk N and Duggan DM, 2002. Energy response of an imaging plate exposed to standard beta sources. *Applied Radiation and Isotopes* 57(6): 875-882

Greilich S, Glasmacher UA and Wagner GA, 2002. Spatially resolved detection of luminescence: a unique tool for archaeochronometry. *Naturwissenschaften* 89(8): 371-375.

Greilich S, Glasmacher UA and Wagner GA, 2005. Optical dating of granitic stone surfaces. *Archaeometry* 47: 645-665.

Hareyama M, Tsuchiya N and Takebe M, 1998. Two-dimensional measurement of natural radioactivity of rocks by photostimulated luminescence. *Water-Rock Interaction*, Rotterdam.

Hareyama M, Tsuchiya N, Takebe M and Chida T, 2000. Two-dimensional measurement of natural radioactivity of granitic rocks by photostimulated luminescence technique. *Geochemical Journal* 34(1): 1-9.

IAEA Report RL 148, 1987. Preparation of Gamma-ray Spectrometry Reference Materials RGU-1, RGTh-1 and RGK-1. *Report – IAEA/RL/148*, Vienna

Lomax J, Hilgers A, Wopfner H, Grün R, Twidale CR and Radtke U, 2003. The onset of dune formation in the Strzelecki Desert, South Australia. *Quaternary Science Reviews* 22(10-13): 1067-1076

Lomax J, Hilgers A, Twidale CR, Bourne JA and Radtke U, 2007. Treatment of broad palaeodose distributions in OSL dating of dune sands from the western Murray Basin, South Australia. *Quaternary Geochronology* 2(1-4): 51-56.

Matsuda T, Arakawa S, Koda K, Torii S and Nakajima N, 1993. New technical developments in the FCR9000. *Fuji Computed Radiography Technical Review* No 2 (Fuji Photo Film)

Mayya YS, Morthekai P, Murari MK and Singhvi AK, 2006. Towards quantifying beta microdosimetric effects in single-grain quartz dose distribution. *Radiation Measurements* 41(7-8): 1032-1039.

Miyahara J, 1989. The Imaging Plate: A new radiation image sensor. *Chemistry Today* No. 223: 29-36

Mori K and Hamaoka T, 1994. IP Autoradiography System (BAS). *Protein, Nucleic Acid and Enzyme* 39(11): 11.

Murray AS and Wintle AG, 2000. Luminescence dating of quartz using an improved single-aliquot regenerative-dose protocol. *Radiation Measurements* 32(1): 57-73.

Nathan RP, Thomas PJ, Jain M, Murray AS and Rhodes EJ, 2003. Environmental dose rate heterogeneity of beta radiation and its implications for luminescence dating: Monte Carlo modelling and experimental validation. *Radiation Measurements* 37(4-5): 305-313

Olley JM, Caitcheon GG and Roberts RG, 1999. The origin of dose distributions in fluvial sediments, and the prospect of dating single grains from fluvial deposits using optically stimulated luminescence. *Radiation Measurements* 30(2): 207-217.

Pickering R, Kramers JD, Partridge T, Kodolanyi J and Pettke T, 2009. Uranium-lead dating of calcite-aragonite layers in low-uranium speleothems from South Africa by MC-ICP-MS. *Quaternary Geochronology*, accepted manuscript

Preusser F, Blei A, Graf H and Schlüchter C, 2007. Luminescence dating of Wurmian (Weichselian) proglacial sediments from Switzerland: methodological aspects and stratigraphical conclusions. *Boreas* 36(2): 130-142.

Rowlands JA, 2002. The physics of computed radiography. *Physics in Medicine and Biology* 47(23): R123-R166.

Salis M, 2003. On the photo-stimulated luminescence of BaFBr : Eu+2 phosphors. *Journal of Luminescence* 104(1-2): 17-25

Schweizer S, 2001. Physics and current understanding of X-ray storage phosphors. *Physica Status Solidi a - Applied Research* 187(2): 335-393.

Seibert JA, 1997. Computed radiography: technology and quality assurance. In: Frey GD and Sprawls P, eds, *The Expanding Role of Medical Physics in Diagnostic Imaging for AAPM*. Madison: Advanced Medical Publishing. 37-83

Spaeth JM, 2001. Recent developments in X-ray storage phosphor materials. *Radiation Measurements* 33(5): 527-532.

Takahashi K, 2002. Progress in science and technology on photostimulable BaFX : Eu2+ (X = Cl, Br, I) and imaging plates. *Journal of Luminescence* 100(1-4): 307-315.

Tanaka KA, Yabuuchi T, Sato T, Kodama R, Kitagawa Y, Takahashi T, Ikeda T, Honda Y and Okuda S, 2005. Calibration of imaging plate for high energy electron spectrometer. *Review of Scientific Instruments* 76(1).

Thoms M, 1996. The quantum efficiency of radiographic imaging with image plates. *Nuclear Instruments & Methods in Physics Research Section a-Accelerators Spectrometers Detectors and Associated Equipment* 378(3): 598-611.

Tsuchiya N and Hareyama M, 2001. Two-dimensional measurement of natural radioactivity of some Archean and Proterozoic rocks from South Africa. *Memoirs. National Institute of Polar Research* (Special Issue 55): 167-177.

Vandenberghe D, Hossain SM, De Corte F and Van den Haute P, 2003. Investigations on the origin of the equivalent dose distribution in a Dutch coversand. *Radiation Measurements* 37(4-5): 433-439.